JACS
JOURNAL OF THE AMERICAN CHEMICAL SOCIETY
pubs.acs.org/JACS
Article

Optical Kerr Effect of Liquid Acetonitrile Probed by Femtosecond Time-Resolved X-ray Liquidography

Hosung Ki,[▽] Seungjoo Choi,[▽] Jungmin Kim, Eun Hyuk Choi, Seonggon Lee, Yunbeom Lee, Kihwan Yoon, Chi Woo Ahn, Doo-Sik Ahn, Jae Hyuk Lee, Jaeku Park, Intae Eom, Minseok Kim, Sae Hwan Chun, Joonghan Kim, Hyotcherl Ihee,* and Jeongho Kim*

Cite This: J. Am. Chem. Soc. 2021, 143, 14261−14273

ABSTRACT: Optical Kerr effect (OKE) spectroscopy is a method that measures the time-dependent change of the birefringence induced by an optical laser pulse using another optical laser pulse and has been used often to study the ultrafast dynamics of molecular liquids. Here we demonstrate an alternative method, femtosecond time-resolved X-ray liquidography (fs-TRXL), where the microscopic structural motions related to the OKE response can be monitored using a different type of probe, i.e., X-ray solution scattering. By applying fs-TRXL to acetonitrile and a dye solution in acetonitrile, we demonstrate that different types of molecular motions around photoaligned molecules can be resolved selectively, even without any theoretical modeling, based on the anisotropy of two-dimensional scattering patterns and extra structural information contained in the q-space scattering data. Specifically, the dynamics of reorientational (libration and orientational diffusion) and translational (interaction-induced motion) motions are captured separately by anisotropic and isotropic scattering signals, respectively. Furthermore, the two different types of reorientational motions are distinguished from each other by their own characteristic scattering patterns and time scales. The measured time-resolved scattering signals are in excellent agreement with the simulated scattering signals based on a molecular dynamics simulation for plausible molecular configurations, providing the detailed structural description of the OKE response in liquid acetonitrile.

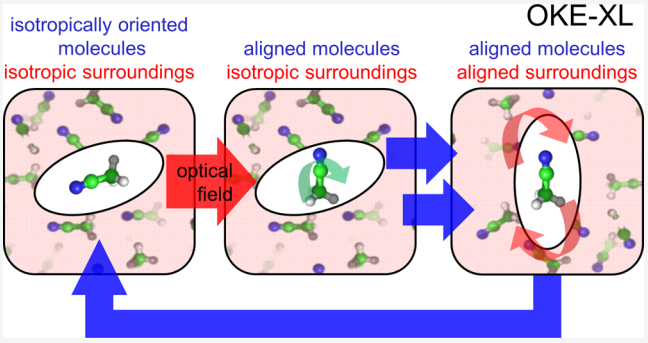

INTRODUCTION

When a strong linearly polarized light interacts with a material, it induces birefringence, that is, different indices of refraction in two perpendicular directions with respect to the light polarization. Such a change in the refractive index of a material in response to the applied light is called the optical Kerr effect (OKE).[1−4] Since the OKE is responsible for nonlinear optical effects such as self-focusing and self-phase modulation, it has been used for laser applications such as mode-locking of femtosecond lasers.[5] In molecular spectroscopy, OKE has been used as a tool to investigate the dynamics of molecular liquids, so-called OKE spectroscopy.[3,6−10] In OKE spectroscopy, the ultrafast response of a material to a perturbation (birefringence) generated by an external stimulus (optical laser pulse) is monitored to provide information on the microscopic mechanism underlying the relaxation of transient birefringence generated in the material.[1,3,6,8,10] Over many decades, OKE spectroscopy has been used to investigate the ultrafast dynamics of orientational motions and intramolecular and intermolecular vibrations in molecular liquids as well as their connection to solvation dynamics.[8,11−17]

From previous OKE studies of molecular liquids, it has been revealed that the following three different types of molecular motions contribute to the ultrafast OKE response of molecular liquids: libration, interaction-induced motion, and orientational diffusion, in the chronological order of appearance.[6−8,18,19] Libration is a rocking motion arising from the rotational motion obstructed by the surrounding cage molecules, and the collective librational motions of liquid molecules have been regarded to account for the initial fast OKE response on the time scale from sub-100 to 200 fs. Interaction-induced motion has been known to contribute to the OKE signal on the intermediate time scale ranging from sub-picoseconds to picoseconds.[7,20,21] Orientational diffusion is a rather slow collective rotation of individual molecules and is responsible for the slow decay of the OKE signal on the

Received: June 12, 2021
Published: August 30, 2021

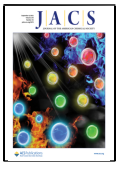

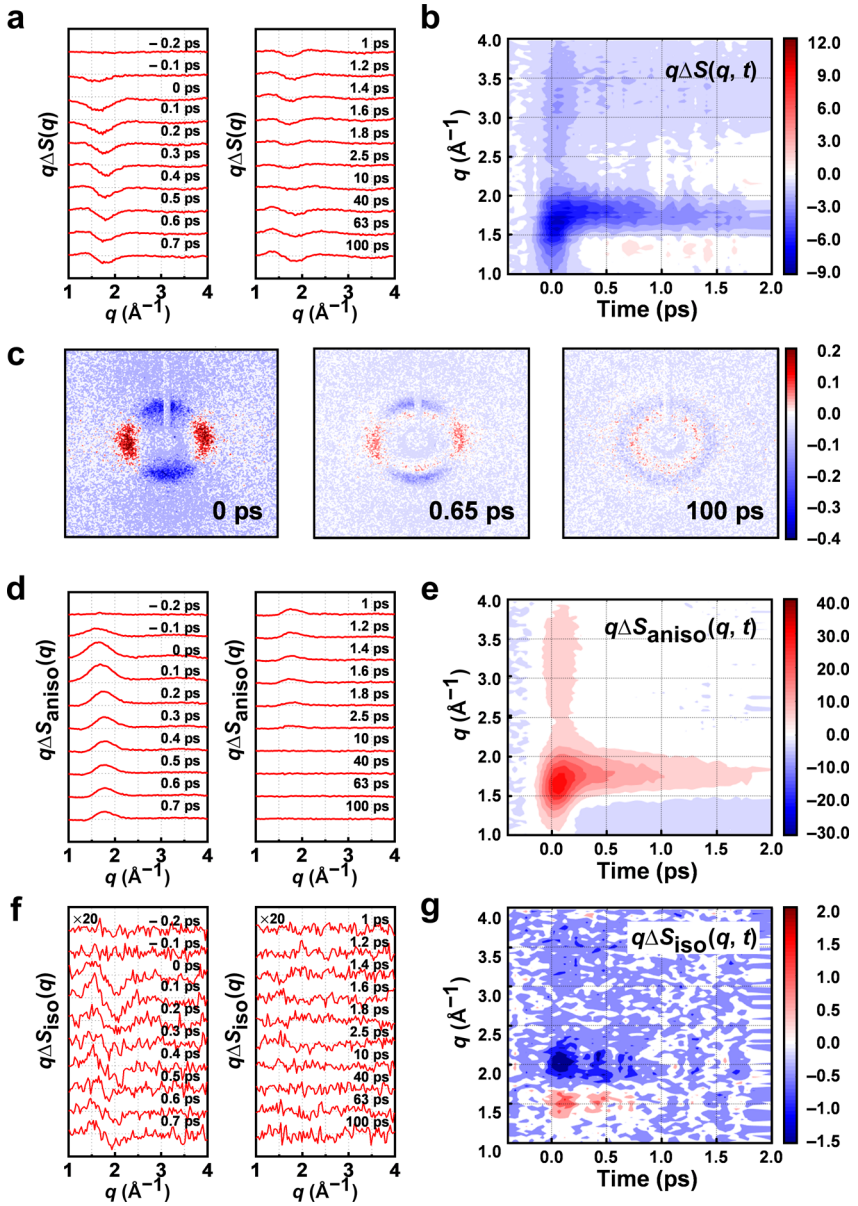

Figure 1. TRXL signals of the dye solution in acetonitrile. (a) Difference scattering curves at individual time delays and (b) their contour plot in the early time range. Difference scattering curves, $\Delta S(q, t)$, were multiplied by the magnitude of the momentum-transfer vector, q, to give $q\Delta S(q, t)$ so that the signals at large q-values are emphasized. (c) Experimental 2D difference scattering images at three representative time delays of 0, 0.65, and 100 ps. (d) Anisotropic scattering components at individual time delays and (e) their contour plot in the early time range. Anisotropic scattering components, ΔS_{aniso}, are multiplied by the magnitude of the momentum-transfer vector, q, to give $q\Delta S_{aniso}$ so that the signals at large q-values are emphasized. (f) Isotropic scattering components at individual time delays and (g) their contour plot in the early time range. Isotropic scattering components, ΔS_{iso}, are multiplied by the magnitude of the momentum-transfer vector, q, to give $q\Delta S_{iso}$ so that the signals at large q-values are emphasized. Note that, for $q\Delta S_{iso}$ shown in this figure, the contribution of thermal heating was removed from the raw $q\Delta S_{iso}$ shown in Figure S5.

picosecond time scale. These assignments of the molecular motions associated with the OKE signal on various time scales rely on theoretical simulations, such as a molecular dynamics (MD) simulation combined with instantaneous normal mode (INM) analysis,[18,19,22−26] rather than the direct observation of the motions in real space mainly due to the lack of an experimental means to directly visualize the evolution of the collective molecular rearrangement in solution. In fact, instead of the molecular-level theoretical simulations, analytical methods based on theoretical models such as the mode-coupling theory,[27] Kubo's discrete random jump model, and the multimode Brownian oscillator model have also been developed.[28] For example, with the method based on the mode-coupling theory, OKE spectroscopy data measured at a series of different temperatures can be analyzed to specify vibrational modes contributing to the structural relaxation following the OKE.[28,29] However, despite the many advantages of the kinetic analysis based on these theoretical models, these methods cannot directly provide molecular-level structural information on the assigned kinetic components because the underlying theoretical models lack the microscopic structural details and rather focus on the phenomenological or mesoscopic description of the observed kinetics. In this regard, it would be desirable to employ a structurally sensitive probe,

https://doi.org/10.1021/jacs.1c06088
J. Am. Chem. Soc. 2021, 143, 14261−14273

instead of an optical probe, in a time-resolved measurement so that molecular motions associated with the relaxation of macroscopic birefringence can be directly probed in real space.

Femtosecond time-resolved X-ray liquidography (fs-TRXL), which is also known as femtosecond time-resolved X-ray solution scattering (fs-TRXSS), would be an appropriate tool for probing the molecular dynamics that result from the OKE. In a fs-TRXL experiment, a femtosecond optical pulse is used as a pump, and the X-ray scattering of a femtosecond X-ray pulse generated from an X-ray free-electron laser (XFEL) is used as a probe.[30−37] Compared with conventional OKE spectroscopy that employs an all-optical pump−probe scheme, fs-TRXL provides superior structural sensitivity to the global molecular structure and therefore has been used to investigate the structural dynamics of chemical and biological reactions in the liquid solution phase.[30,31,33,34,37−49] While the time resolution of the time-resolved X-ray liquidography (TRXL) experiment had been previously limited by ∼100 ps X-ray pulses generated from third-generation synchrotrons, the development of XFEL has allowed us to probe the ultrafast dynamics on femtosecond time scales using TRXL.

In this work, we present a fs-TRXL measurement to visualize the molecular motions associated with the OKE. The measured TRXL data consist of anisotropic two-dimensional (2D) scattering patterns, which can be decomposed into the anisotropic and isotropic signals.[31,33,45,48,50,51] The anisotropic and isotropic signals, which are more sensitive to the change of the orientations of molecules and the change of the intermolecular distance, respectively, show different characteristic scattering patterns and time scales. To account for the structural origin of the ultrafast scattering signal, we reproduced the experimental time-resolved X-ray solution scattering curves of the pure solvent with the aid of a molecular dynamics (MD) simulation on a model system, which resembled the liquid environment that was perturbed by an optical pulse and subsequently relaxed orientationally. Based on the time scales of the decay dynamics and the scattering patterns of ultrafast TRXL signal in comparison with the theoretical scattering patterns calculated from the MD simulation, we can attribute the ultrafast TRXL signal to the relaxation of OKE and identify the molecular configurations associated with the relaxation dynamics. The anisotropic scattering signal, which is inherently sensitive to orientational motions, exhibits the dynamics of libration and orientational diffusion. In contrast, the isotropic scattering signal shows the interaction-induced dynamics, indicating that this motion involves the change of interatomic distances rather than orientational changes.

RESULTS AND DISCUSSION

We performed a fs-TRXL measurement at an XFEL on a solution of dye, 4-bromo-4′-(*N*,*N*-diethylamino)-azobenzene, in acetonitrile. For the pump pulse, we used a 100 fs optical laser pulse at 400 nm that is resonant with the electronic absorption of the dye. The detailed protocol for the experiment is described in the Experimental Section. The measured TRXL signals, $\Delta S(q, t)$, are the difference between the azimuthally averaged laser-on and laser-off signals and are represented in terms of (i) the magnitude of the momentum-transfer vector, $q = (4\pi/\lambda)\sin(2\theta/2)$, where λ is the X-ray wavelength and 2θ is the scattering angle, and (ii) the time delay, t, between the optical laser pulse and the X-ray pulse. $\Delta S(q, t)$ signals of the dye solution are shown in Figures 1a and b. The photoexcitation energy absorbed by the dye molecule is dissipated to the surrounding solvent molecules, leading to the changes in the temperature and density, and consequently the change of the X-ray scattering pattern, on the time scales from tens of picoseconds to microseconds. The solvent heating signal of the dye solution measured at a 100 ps time delay has already been well characterized by TRXL measurements at synchrotrons, which gives the time resolution of ∼100 ps.[52,53] In our fs-TRXL measurement at the XFEL, the solvent heating signal at the 100 ps time delay was well reproduced. Besides the change of the temperature of the solvent, $\Delta S(q, t)$ signals of the dye solution show an ultrafast response that grows following the instrument response function (IRF), which is ∼200 fs, and decays on a picosecond time scale, as can be seen in Figures 1a and b. The q-space profile of the ultrafast response is clearly different from that of the solvent heating signal, which is shown in Figure S1 in the Supporting Information (SI).

As shown in Figure 1c, the 2D scattering images measured at positive time delays are significantly anisotropic. Such anisotropy is often observed when linearly polarized light is used as the pump for the TRXL measurement on solution samples that contain solutes resonant with the pump light due to the preferential excitation of solute molecules with transition dipoles oriented along the polarization direction of the pump light. To obtain more detailed information on the origin of the TRXL signals, we decomposed the anisotropic scattering images into the isotropic scattering component, $\Delta S_{iso}(q, t)$, and the anisotropic scattering component, $\Delta S_{aniso}(q, t)$, using a linear regression fitting with the following equation:[31,33,45,48,54−56]

$$\Delta S(q, t, \theta_q) \propto \Delta S_{iso}(q, t) - P_2(\cos(\theta_q))\cdot\Delta S_{aniso}(q, t) \quad (1)$$

where θ_q is the angle between the linear laser polarization direction and the momentum transfer vector ($\boldsymbol{q}$) for the X-ray scattering and $P_2(x)$ is the second-order Legendre polynomial, that is, $1/2(3x^2 - 1)$. According to eq 1, $\Delta S_{aniso}(q, t)$ and $\Delta S_{iso}(q, t)$ represent the scattering signals of molecules with anisotropic and isotropic angular distributions, respectively, with respect to the laser polarization direction. Therefore, $\Delta S_{aniso}(q, t)$ is more sensitive to the change of the orientations of molecules and $\Delta S_{iso}(q, t)$ is more sensitive to the change of the inter- or intramolecular atomic-pair distances.

In general, the TRXL signal of a solution sample arises from the following three types of structural changes: (i) the structural change of the solute, (ii) the change of the solvation cage caused by the solute−solvent interaction, and (iii) the response of the bulk solvent.[49] Accordingly, in the dye solution that we used, the observed ultrafast response can arise from (i) the change of the molecular structure of the dye molecules, (ii) the change of the cage structure around the photoexcited dye molecules (that is, solvation), and (iii) the change of the temperature and density of bulk solvent, which is the response of the bulk solvent to the heat dissipation from the photoexcited dye molecules. Since the contribution of the photoinduced structural changes of the dye molecules without any heavy atoms to the difference scattering signal is known to be negligibly small,[53,57] it should not be related to the ultrafast response observed in the TRXL signal of the dye solution. Unlike the molecular structure, the dipole moment of the dye molecule is significantly increased by the photoexcitation to its electronically excited state, as shown in Table S1. In response

https://doi.org/10.1021/jacs.1c06088
J. Am. Chem. Soc. 2021, 143, 14261−14273

to the change of the dipole moment of the solute, solvent molecules surrounding the photoexcited solute molecules are rearranged[11,36,58−62] and thus can contribute to the ultrafast response of the TRXL signal. Previously, such photoinduced solvation in liquid solutions has been intensively studied in the field of solvation dynamics using time-resolved spectroscopy.[8,11,15−19,22,23,58−64] The temperature and density of the bulk solvent would also change in the dye solution, but the q-space profile of the TRXL signal arising from such a change is well characterized from the previous TRXL studies and therefore can be separated from other contributions, as will be discussed later. In addition to the above contributions, the transient alignment of solvent molecules by interactions with the polarized electric field of optical pump pulse, which is known to be the origin of the OKE phenomenon,[3,6−9,65] can also contribute to the ultrafast response of the TRXL signal of the dye solution (and even the neat solvent), as will be discussed below.

To determine the origin of the observed ultrafast response, we also performed a fs-TRXL experiment on neat acetonitrile (that is, without any dye solute), as shown in Figure S2a and b. As shown in Scheme 1, only a single type of solvent response, that is, the OKE response of the bulk solvent molecules, can contribute to the TRXL signal of neat acetonitrile, which does not contain any solute molecule. In contrast, two different types of solvent responses can contribute to the TRXL signal of the dye solution: (i) the solvation of photoexcited dye molecules and (ii) the OKE response of the bulk solvent molecules. By comparing the TRXL signals of the dye solution and those of the neat acetonitrile, the identity of the solvent responses that contribute to the observed TRXL signal of the dye solution can be distinguished from each other. For example, if the two TRXL signals are almost identical to each other, the OKE response of the bulk solvent molecules, which can contribute to both signals, would dominantly contribute to the TRXL signal of the dye solution. On the other hand, if the two TRXL signals are significantly different from each other, the solvation of photoexcited dye molecules would contribute significantly. We note that at early time delays, as shown in Figure S3, the TRXL signal of the neat solvent exhibits similar profiles in both time- and q-domains as those of the TRXL signal of dye solution. From the similarity of the early-time TRXL signals of the dye solution and neat acetonitrile, we can infer that the OKE response of the bulk solvent is a major component contributing to the ultrafast response of TRXL signal of dye solution. While we can intuitively expect that the solvation process following the photoinduced dipole moment change of the solute molecules also contributes to the ultrafast TRXL signal, such a contribution from the solvation of the photoexcited dye molecules was found to be negligible under our experimental conditions, as will be discussed later, mainly because the number of solute molecules is much smaller than the number of solvent molecules and the amplitude of the TRXL signal is proportional to the number density of the probed molecules. In addition, we can see that both ΔS_{iso} and ΔS_{aniso} decay almost completely within 2 ps, as shown in Figure 1d −g. This time scale is much shorter than that for the orientational diffusion of the azobenzene-derivative dye molecule, which rotates in tens of picoseconds.[66,67] The absence of such a slow decay in the observed TRXL signal further supports that the solvation of the photoexcited dye molecules gives only a negligible contribution to the ultrafast decay of the TRXL signal. Thus, from now on we will term the ultrafast response of TRXL signals of the liquid solution and the neat solvent that were investigated in this work as OKE X-ray liquidography (OKE-XL) signals. In fact, similar TRXL signals arising from the OKE response of molecular liquids were recently reported for aqueous solutions.[31,35,48] However, in those studies the contributions of rotational motions of the water molecules were obscured in the measured OKE-XL signal because the X-ray scattering cross-section of hydrogen atoms of water molecules is negligibly small. Accordingly, the observed OKE-XL signals were analyzed in terms of only the translational motion of water molecules.[35]

$\Delta S_{aniso}(q, t)$ and $\Delta S_{iso}(q, t)$ signals of the dye solution are shown in Figure 1d and e and Figure 1f and g, respectively. It can be seen that $\Delta S_{aniso}(q, t)$ and $\Delta S_{iso}(q, t)$ are distinctively different from each other in both the time domain and the q-domain. Notably, $\Delta S_{aniso}(q, t)$ is much larger than $\Delta S_{iso}(q, t)$. Such dominance of $\Delta S_{aniso}(q, t)$ over $\Delta S_{iso}(q, t)$ suggests that the structural changes associated with the light-triggered response in the dye solution mainly consist of the change of the molecular orientations. We note that the $\Delta S_{aniso}(q, t)$ and $\Delta S_{iso}(q, t)$ signals of neat acetonitrile shown in Figure S2 are similar to those of the dye solution.

Besides the ultrafast response, that is, the OKE-XL signal, the TRXL signal of the dye solution contains the contribution of solvent heating induced by the heat dissipation from the

Scheme 1. Schematic of Molecular Movements That Can Contribute to the TRXL Signals of the Neat Solvent and the Dye Solution[a]

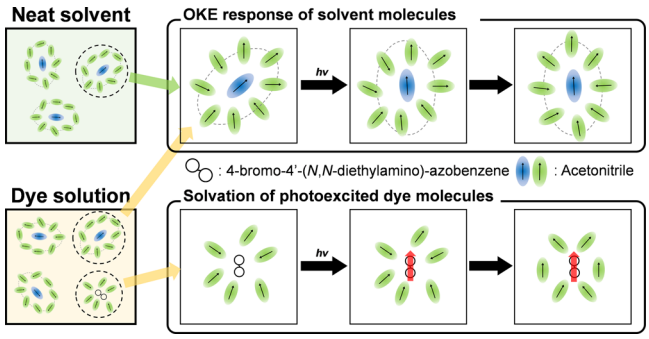

[a]In this work, both the neat solvent and the dye solution were studied to better understand the origin of the ultrafast TRXL signals. We note that the polarization of the excitation light used for the TRXL experiment is assumed to be in the vertical direction in this figure. In the case of the neat solvent, only the OKE response of solvent molecules (upper right panel) can contribute to the TRXL signal of the neat solvent because there is no dye molecule that can absorb light. In contrast, additional molecular movements can occur in the dye solution, including the solvation of photoexcited dye molecules (lower right panel). The red arrow in the lower right panel indicates the direction of the dipole moment of the photoexcited dye molecule. We note that, in addition to the two types of molecular movements depicted in this scheme, other processes also can occur upon the irradiation of light to the dye solution, for example, the photoinduced structural change of dye molecules and the thermal response of the solvent molecules due to heat dissipation from the photoexcited dye molecules. These are omitted from this scheme because their contribution to the TRXL signal is negligibly small (the photoinduced structural change of the dye molecule) and they are not of primary interest in this work (the thermal response of the solvent molecules). We note that the photoinduced structural change of the dye molecule itself has a relatively negligible contribution due to the lack of heavy atoms.

https://doi.org/10.1021/jacs.1c06088
J. Am. Chem. Soc. 2021, 143, 14261−14273

photoexcited dye molecules. Specifically, the scattering curve at a 100 ps time delay represents the change of scattering that arises from the increase of the solvent temperature. Because the heat dissipation is supposed to occur isotropically, the solvent heating contribution should be manifested only in $\Delta S_{iso}(q, t)$ and not in $\Delta S_{aniso}(q, t)$. As shown in Figure S4 from the temporal amplitude profile of the solvent-heating scattering curve manifested in $\Delta S_{iso}(q, t)$, the increase of the solvent temperature was determined to occur biexponentially with time constants of 0.9 ± 1.4 and 45 ± 150 ps. Because the change of the solvent temperature should not be related to the OKE response, we excluded the contribution of solvent heating from our kinetic analysis by subtracting it from the experimental data using the SANOD method.[68] $\Delta S_{iso}(q, t)$ shown in Figure 1f and g corresponds to the scattering curves with the solvent heating contribution eliminated and is different from the raw $\Delta S_{iso}(q, t)$ data shown in Figure S5.

To examine the kinetics of the OKE-XL signal, we first analyzed the temporal behavior of $\Delta S_{iso}(q, t)$ and $\Delta S_{aniso}(q, t)$, as shown in Figure 2. For the kinetic analysis of $\Delta S_{aniso}(q, t)$,

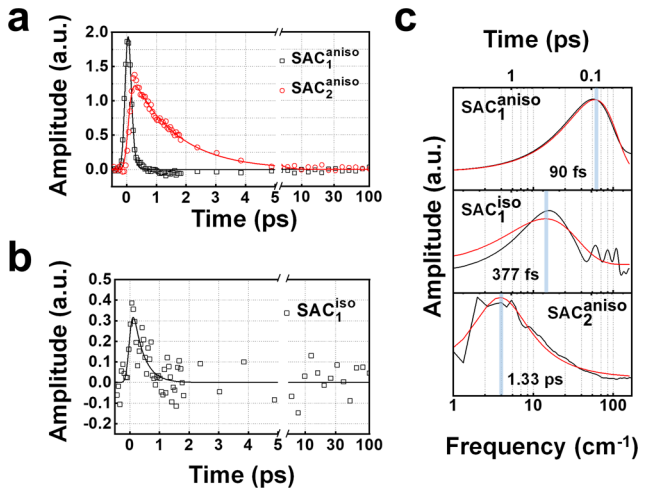

Figure 2. Temporal amplitude profiles of state-associated difference X-ray scattering curves (SACs) of the dye solution in acetonitrile and their FT spectra. Temporal amplitude profiles (dots) of (a) the anisotropic SACs and (b) the isotropic SAC with their theoretical fits (lines) shown together. The shape of each SAC in q-space is shown in Figure 3. The details of the fitting procedure are described in the Supporting Information. The time constants of the decay exponentials were determined to be 60 ± 35 fs for SAC_1^{aniso} (black), 1.5 ± 0.5 ps for SAC_2^{aniso} (red), and 350 ± 210 fs for SAC_1^{iso} (black). (c) FT spectra (black) of temporal amplitude profiles of SACs. The fits (red) of each FT spectrum by a line shape model function[7] are shown together. The details of the fitting procedure are described in the Supporting Information. The peak positions in the FT spectra are indicated by blue vertical bars. The time axis, which was obtained by the conversion of its corresponding frequency axis shown at the bottom, is shown at the top.

we applied the singular value decomposition (SVD) and SVD-aided pseudo principal-component analysis (SAPPA).[69] The detailed procedure for this kinetic analysis is described in the SI in the Kinetic Analysis section and Figure S6. By applying SAPPA, we obtained state-associated difference X-ray scattering curves (SACs), each of which is the difference X-ray scattering curve of a certain transient state and is an analogue of the species-associated spectrum (SAS) or decay-associated spectrum (DAS), which are often used in the data analysis of transient absorption spectroscopy. As can be seen in Figure 3a, two SACs on two different time scales were obtained from the SAPPA of $\Delta S_{aniso}(q, t)$: SAC_1^{aniso} near time zero and SAC_2^{aniso} for at 0.65 ps, which correspond to two transient states. For $\Delta S_{iso}(q, t)$, only a single SAC, SAC_1^{iso}, was obtained directly from the SVD analysis of $\Delta S_{iso}(q, t)$. The temporal amplitude profiles of all the SACs are shown in Figure 2a and b. Notably, the decay rates of the amplitudes of these SACs are different from each other. The amplitude of SAC_1^{aniso} decays rapidly on the sub-100 fs time scale. By contrast, the amplitudes of SAC_2^{aniso} and SAC_1^{iso} decay much more slowly on picosecond and sub-picosecond time scales, respectively.

To determine the decay rates of the SACs quantitatively, we tried two different approaches. First, we fitted the temporal amplitude profiles of the SACs by a pair of rise and decay exponentials that were convoluted with the IRF (~220 ± 40 fs) of the TRXL measurement based on a kinetic model, as shown in Figure 2a and b. The details of the kinetic model used for the fitting are described in the Supporting Methods section. From the analysis of two anisotropic SACs, SAC_1^{aniso} and SAC_2^{aniso}, we identified two time constants, 60 ± 35 fs and 1.5 ± 0.5 ps, respectively. The analysis of the isotropic SAC, SAC_1^{iso}, yielded another different time constant of 350 ± 210 fs. Second, we performed FT line shape analysis, which has been used to investigate the OKE response in previous spectroscopic studies.[7,9,11,65,70−73] For the FT line shape analysis, the temporal amplitude profiles of the SACs were Fourier transformed as shown in Figure 2c. In principle, these Fourier transform spectra (imaginary part) give the decay rates of the SAC amplitude; specifically, the peak positions in these spectra correspond to the decay rates of the major kinetic components. Then, we fitted each FT spectrum by a line shape model function to obtain the decay rate of the kinetic component manifested in each SAC. As can be seen in Figure 2c from the FT line shape analysis, the time constants for the decays of SAC_1^{aniso}, SAC_1^{iso}, and SAC_2^{aniso} were obtained to be 90 fs, 377 fs, and 1.33 ps, respectively. In addition, we also applied the FT line shape analysis to the raw data of $\Delta S_{aniso}(q, t)$ and $\Delta S_{iso}(q, t)$, as shown in Figure S7. Specifically, by performing the FT line shape analysis on the temporal profiles of $\Delta S_{aniso}(q, t)$ and $\Delta S_{iso}(q, t)$ at several selected q-values, we obtained two decay time constants (~100 fs and ~1 ps) for $\Delta S_{aniso}(q, t)$ and one decay time constant (~300 fs) for $\Delta S_{iso}(q, t)$, which agree well with the kinetics determined from the FT line shape analysis of the SACs. Overall, the time constants obtained from the two different approaches, namely, fitting using rise and decay exponentials and FT line shape analysis, are in excellent agreement. A notable point from the kinetic analysis is that the anisotropic and isotropic signal components exhibit completely independent kinetic behaviors; there is no common kinetic time constants for the anisotropic and isotropic signal components.

From the kinetic analysis of the two anisotropic SACs, SAC_1^{aniso} and SAC_2^{aniso}, we identified the following two states: (i) a photoaligned state and (ii) an intermediate state (termed the first intermediate state). From the kinetic analysis of the isotropic SAC, SAC_1^{iso}, we identified (iii) another intermediate state (termed the second intermediate state). The photoaligned state is impulsively formed from the (randomly oriented) equilibrium state within the time scale of IRF and converted to the first intermediate state with a 60 ± 35 fs time constant. Subsequently, the first intermediate state is converted back to the equilibrium state with a 1.5 ± 0.5 ps time constant.

https://doi.org/10.1021/jacs.1c06088
J. Am. Chem. Soc. 2021, 143, 14261−14273

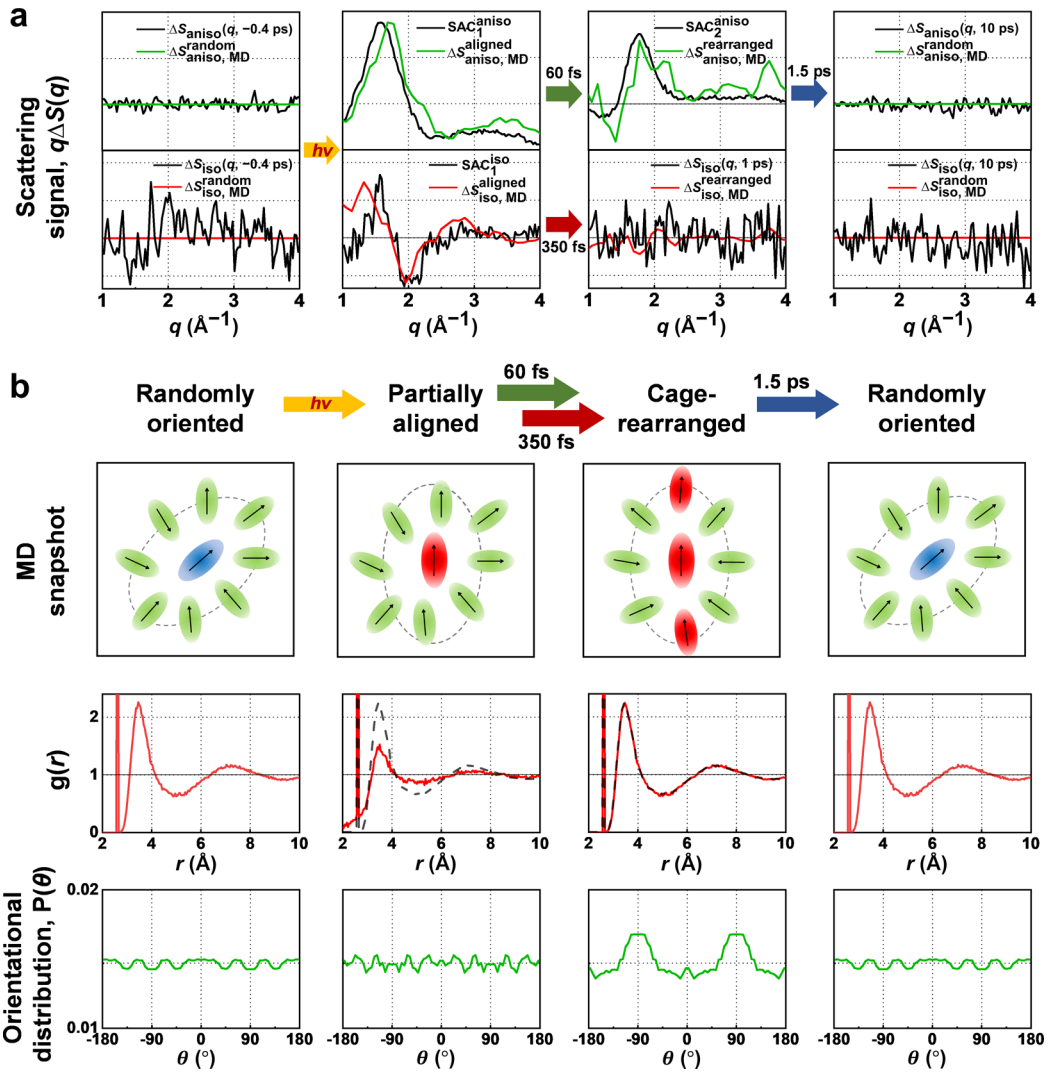

Figure 3. Comparison of experimental difference scattering curves from the TRXL measurement on the dye solution and theoretical difference scattering curves calculated from MD simulations of photoaligned liquid acetonitrile molecules. (a) Anisotropic (top) and isotropic (bottom) components of experimental difference scattering curves or SACs (black) are compared with the corresponding theoretical scattering curves (green or red) calculated from MD snapshots for the partially aligned, cage-rearranged, and randomly oriented configurations. The time constants obtained from the temporal amplitude profiles of SACs are shown between the plots. (b) The schematic of representative MD snapshots (top row), the radial distribution functions (RDFs) of the methyl carbon−nitrogen pairs of all the acetonitrile molecules (middle row), and the orientational distribution functions (ODFs) of cage molecules surrounding the aligned molecules (bottom row) are described for the randomly oriented configuration (first and last columns), the partially aligned configuration (second column), and the cage-rearranged configuration (third column). In the schematic of MD snapshots, only the solvent molecules are represented, and the dye solute molecules are not shown because the dye molecules do not significantly contribute to the measured TRXL signal. The direction of laser polarization was set to be $\theta = 90°$ and $\theta = -90°$ and the molecular alignment was made accordingly along that direction. The time constants obtained from the experimental OKE-XL data are shown between the configurations for easier comparison with the experimental data.

The second intermediate state is formed with a time constant of 350 ± 210 fs. When comparing the time scales for the formation of the first and second intermediate states, we can infer that the second intermediate state must be formed from the first intermediate state; however, each intermediate state is identified in only one of the isotropic and anisotropic signals. This observation indicates that the molecular motions leading to the formation of the first and the second intermediates states are of different characters. From the OKE-XL signals of neat acetonitrile, as shown in Figure S8, kinetic components similar to those of the dye solution were identified as follows: 52 ± 7 fs for SAC_1^{aniso}, 1.8 ± 0.6 ps for SAC_2^{aniso}, and 150 ± 170 fs for SAC_1^{iso}. However, it should be noted that the formation of the second intermediate state is substantially faster in neat acetonitrile (150 fs) than in the dye solution (350 fs), as will be discussed later.

For a comparison of the kinetics determined from the OKE-XL signal with the kinetics reported in previous spectroscopic and theoretical studies on the OKE, the time constants for various types of motions involved in the OKE response as determined from the literature are listed in Table S2. We note that, for consistency, we performed the same kinetic analysis of our own on the previously published spectroscopic data to obtain the time constants shown in Table S2 rather than showing the reported values (presumably determined with different analysis methods or even not determined) from the literature. Based on these time constant values, we can assign the kinetic components identified from the OKE-XL signals

https://doi.org/10.1021/jacs.1c06088
J. Am. Chem. Soc. 2021, 143, 14261−14273

presented in this work. The 60 fs kinetic component of the anisotropic OKE-XL signal agrees well with the time scales of the initial fast decay component of the OKE spectroscopic signal of neat acetonitrile (74[6] and 79 fs[7], respectively). As in those previous studies, this ultrafast kinetic component can be assigned to the libration of liquid molecules. The 1.5 ps kinetic component of the anisotropic OKE-XL signal is in good agreement with the slow decay component of the OKE spectroscopic signal of neat acetonitrile (1.64[6] and 1.43 ps[7], respectively) and can be assigned to the orientational diffusion of liquid molecules. The 350 fs kinetic component of the isotropic OKE-XL signal well matches the intermediate decay component of the OKE spectroscopic signal of neat acetonitrile (225[6] and 222 fs[7], respectively) and can be assigned to the interaction-induced motion of liquid molecules. Based on this assignment of the kinetic components observed in the OKE-XL data, we can make a kinetic model as follows: the photoaligned state impulsively formed by optical pump pulse is converted to the first intermediate state with a time constant of 60 fs via libration. Subsequently, the first intermediate state is converted to the second intermediate with a time constant of 350 fs via the interaction-induced motion. Finally, the second intermediate relaxes back to the equilibrium state with a 1.5 ps time constant via orientational diffusion.

In Figure S9, $\Delta S_{aniso}(q, t)$ data of the dye solution and neat acetonitrile are compared, and it can be seen that their shapes and temporal dynamics are nearly identical to each other. The similarity of $\Delta S_{aniso}(q, t)$ data of the dye solution and those of the neat solvent implies that the anisotropic component of OKE-XL signals of both the solution and the neat solvent arise from the same structural origin, that is, the OKE response of the solvent. Since a dilute sample solution mainly consists of solvent molecules with only a small portion of solute molecules, and the amplitude of the TRXL signal is proportional to the number density of probed molecules, it is reasonable that the TRXL signal is dominated by the OKE response of the solvent.

In Figure S10, $\Delta S_{iso}(q, t)$ data of the dye solution and neat acetonitrile are compared. While they have identical shapes in q-space, the amplitude and temporal dynamics of $\Delta S_{iso}(q, t)$ are different for the dye solution and neat acetonitrile, which is in contrast to $\Delta S_{aniso}(q, t)$. Specifically, $\Delta S_{iso}(q, t)$ of the dye solution has a much larger amplitude than that of neat acetonitrile. Since the isotropic signal arises from the interaction-induced motion, this observation suggests that the contribution of interaction-induced motion is much larger in the dye solution than in neat acetonitrile, which is in agreement with the result of a previous study using time-resolved OKE spectroscopy.[7] From time-resolved OKE spectroscopic measurements on a dye (Coumarin 153) in chloroform or acetonitrile, it was shown that the overall amplitude of the OKE spectroscopic signal of the dye solution increases with the concentration of dyes in solution.[7,74,75] In particular, in acetonitrile the contribution of interaction-induced motion (compared with the contributions of libration and orientational diffusion) increases most significantly with the concentration of the solution, presumably due to the dipole−dipole nature of the interaction between the dye and acetonitrile molecules and the much larger electric dipole moment of the excited-state dye compared to that of acetonitrile. Besides, in the comparison of the OKE-XL data of the dye solution and neat acetonitrile we also observed that the intermediate kinetic component (that is, interaction-induced motion) of the dye solution is considerably slower than that of neat acetonitrile (350 versus 150 fs, respectively). The slower dynamics of the interaction-induced motion in the dye solution can be attributed to the larger size and mass of the dye molecule compared to those of the acetonitrile molecule, which would lead to a slower translation for solute−solvent collision in the dye solution. Such a difference in the time scale of the interaction-induced motion in the dye solution and the neat solvent was not clearly resolved in the previous OKE spectroscopic study.[7] In contrast, such a subtle difference in time scales of interaction-induced motion in the dye solution and the neat acetonitrile is resolved by the OKE-XL signal because the contribution of the interaction-induced motion manifests only in $\Delta S_{iso}(q, t)$ and is separated from the contributions of libration and orientational diffusion that manifest in $\Delta S_{aniso}(q, t)$.

In addition to the kinetics in the time domain, the scattering-based TRXL technique provides extra q-space information on the change of the global molecular structure, which is clearly an advantage over time-resolved optical spectroscopy. By taking advantage of this feature, we analyzed the q-space profiles of SACs to decipher what type of motions give rise to the time-resolved scattering patterns observed by TRXL. From this analysis, we can examine whether our assignment of the motions associated with the OKE response based on the temporal behavior of the OKE-XL signal is consistent in real space with the molecular motions predicted by theory. In particular, we tried to determine the molecular configurations of all the states included in our kinetic model with the aid of MD simulations. To do so, we prepared three plausible molecular configurations (MD snapshots) for liquid acetonitrile molecules: (i) the partially aligned configuration corresponding to the photoaligned state, (ii) the cage-rearranged configuration corresponding to the second intermediate, and (iii) the randomly oriented configuration corresponding to the equilibrium state. The first configuration was generated by manually changing the angular orientations of a fraction of molecules that were initially in the randomly oriented configuration to the direction of the laser polarization. The partially aligned configuration represents the molecular configuration where a fraction of molecules is aligned by light along the direction of laser polarization while their surrounding molecules remain intact. The latter two configurations (the cage-rearranged configuration and the randomly oriented configuration) were obtained using the MD simulations. The cage-rearranged configuration represents the molecular configuration where molecules in the cage are rearranged via libration and interaction-induced motions in response to the photoinduced alignment of molecules. The randomly oriented configuration indicates the molecular configuration where all of the molecules are randomly oriented by orientational diffusion. For these two molecular configurations, we performed MD simulations on 539 acetonitrile molecules that were contained in a cubic box of 46.75 nm^3 until each molecular configuration was optimized. The detailed procedure of the MD simulation is described in the SI.

From the MD snapshots of the partially aligned and the cage-rearranged configurations, we calculated theoretical difference scattering curves, $\Delta S^{theory}(q)$, by subtracting the scattering curve calculated for the randomly oriented configuration from the scattering curves calculated for the partially aligned and cage-rearranged configurations. For a

https://doi.org/10.1021/jacs.1c06088
J. Am. Chem. Soc. 2021, 143, 14261−14273

direct comparison with the anisotropic and isotropic SACs extracted from the OKE-XL data, $\Delta S^{\text{theory}}{}_{\text{aniso}}(q)$ and $\Delta S^{\text{theory}}{}_{\text{iso}}(q)$ were calculated separately for each configuration. The resultant theoretical difference scattering curves are compared with the experimental SACs obtained from the OKE-XL data in Figure 3a. The theoretical SACs and the experimental ones are in excellent agreement with each other in terms of their shapes, indicating that the molecular configurations we proposed based on the MD simulation describe the phototriggered collective motions of liquid molecules well.

To gain further insight into the structural changes associated with the OKE response, as shown in Figure 3b, we examined (i) the radial distribution functions (RDFs) of the methyl carbon−nitrogen pair in all the acetonitrile molecules and (ii) the orientational distribution functions (ODFs) of cage molecules surrounding the photoaligned molecules, both of which were calculated from the MD snapshots. The RDF of the randomly oriented configuration oscillates around a value of 1, indicating that a molecule is surrounded by a number of molecules that collectively form a layered shell-like structure. Such a layered shell-like structure is commonly observed in the liquid phase, being called the coordination shell for neat solvents or the solvation shell for liquid solutions.[76−83] In contrast, the RDF of the partially aligned configuration oscillates with a much smaller magnitude and has a broader profile than the RDF of the randomly oriented configuration. The RDF of the partially aligned configuration indicates that the coordination shell (which will be also termed the "cage" hereafter) of the photoaligned molecule is perturbed by the partial alignment of liquid molecules to generate a broadened distribution of intermolecular distances, as described in the schematic MD snapshot for the partially aligned configuration in Figure 3b. The ODFs are flat in both the randomly oriented and partially aligned configurations but clearly have peaks at the orientations of the laser polarization direction, namely, θ = 90° and θ = −90°, in the cage-rearranged configuration. The ODF of the cage-rearranged configuration indicates that the molecules in the coordination shell are reoriented via libration, leading to the alignment of cage molecules along the photoaligned molecules as described in the schematic MD snapshot for the cage-rearranged configuration in Figure 3b. In contrast to the ODF, the RDF of the cage-rearranged configuration is almost identical to that of the randomly oriented configuration, suggesting that the intermolecular distance distribution broadened by the photoinduced alignment of molecules had already relaxed back to the narrower intermolecular distance distribution equivalent to the distribution at equilibrium, although some molecules stayed aligned. Therefore, we can infer that not only the libration but also a translational motion (presumably the interaction-induced motion)[7,24,65,84] contribute to the formation of the cage-rearranged state. Finally, the ODF of the cage-rearranged configuration returns to that of the randomly oriented equilibrium state via the orientational diffusion of both photoaligned and cage molecules. Thus, the changes of RDFs and ODFs reveal that (i) the partial alignment of molecules initially induces the broadening of the RDF and (ii) the subsequent cage rearrangement involves both the libration of cage molecules and the interaction-induced motion of a translational character, leading to the alignment of cage molecules along the photoaligned molecules and the restoration of the equilibrium intermolecular distance distribution.

The results of the TRXL measurement and data analysis using the kinetic analysis and the MD simulation visualize the OKE response of acetonitrile in real space at the molecular level, as described in Figure 4. At equilibrium (without any

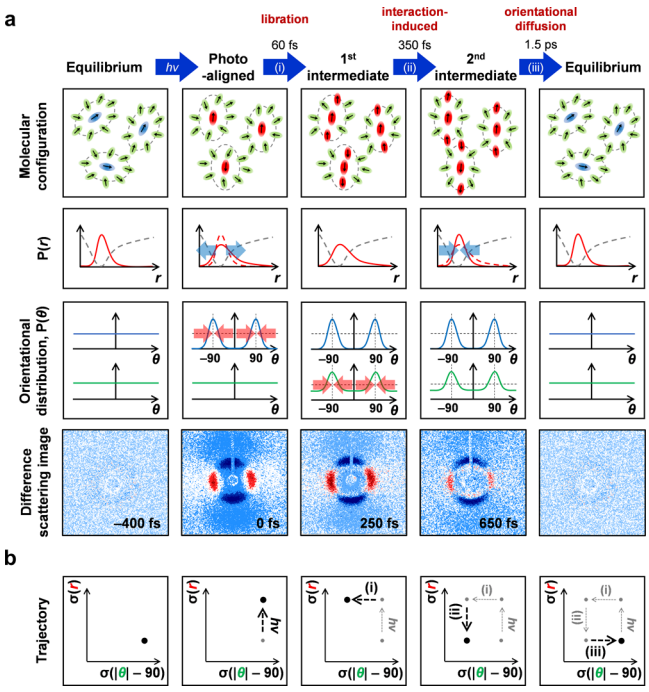

Figure 4. Structural description of the OKE response of liquid acetonitrile. (a) Schematic representation of the molecular configurations (top row) of various states involved in the OKE response of liquid acetonitrile, shown in the chronological order of appearance (from left to right), the population distribution in terms of the intermolecular distance (second row), population distributions in terms of the angular orientation of the photoaligned molecules (upper, blue line) and their cage molecules (lower, green line) (third row), and the representative experimental 2D difference scattering images corresponding to those states (bottom row). In the molecular configurations, the directions of laser polarization were set to be θ = 90° and θ = −90°, and the molecular alignment was made accordingly along those directions. In the second row, the red dashed curves indicate the distribution of the intermolecular distance in a previous state and, for reference, the gray dashed curves indicate the potential energy curve of the ground electronic state of the molecule. (b) Trajectory of the OKE response in terms of the width of the orientational distribution of cage molecules (x-axis) and the width of the distribution of intermolecular distance (y-axis).

interaction with light), the molecules are randomly oriented and thus have an isotropic orientational distribution. Because the molecules are randomly oriented, their surrounding molecules in the coordination shell are also randomly oriented. Accordingly, the ODFs of all the molecules (including molecules that will be aligned by light and their cage molecules) are flat, and the intermolecular distance distribution has the typical shape of a normal distribution. Upon interaction with polarized light, some fraction of the molecules are impulsively aligned along the direction of the laser polarization, yielding a highly anisotropic scattering pattern in the photoaligned state. Accordingly, peaks are formed at θ = 90° and θ = −90° in the ODF of the photoaligned molecules.

https://doi.org/10.1021/jacs.1c06088
J. Am. Chem. Soc. 2021, 143, 14261−14273

Due to the sudden alignment of molecules, the intermolecular distance distribution becomes broader than that in the equilibrium state. However, at this moment the surrounding cage molecules have not yet changed their orientations in response to the photoinduced alignment of the molecules, retaining random orientations. Therefore, the ODF of the cage molecules is still flat. Then, during the transition to the first intermediate state, the cage molecules surrounding the photoaligned molecules rearrange in 60 fs via libration, resulting in the change of the amplitude and the shape of the anisotropic scattering signal (see the 2D difference scattering images at 0 and 250 fs in Figure 4a). As a result, not only the photoaligned molecules but also their cage molecules display anisotropic angular orientations with peaks formed at $\theta = 90°$ and $\theta = -90°$ in the ODF of the cage molecules. However, since libration is primarily of an orientational character,[6,7,61,65] the intermolecular distance distribution remains the same as that in the photoaligned state. During the transition to the second intermediate state, the cage molecules further relax in 350 fs via interaction-induced motion, which changes the interatomic distances rather than the molecular orientation[7,65] and leads to the amplitude change of the isotropic scattering signal (see the 2D difference scattering images at 250 and 650 fs in Figure 4a). Specifically, the intermolecular distance distribution becomes narrower to be equivalent to that of the initial equilibrium state, whereas the ODF remains unchanged. Finally, the anisotropic orientations of the photoaligned molecules and their cage molecules become randomized with a 1.5 ps time constant via orientational diffusion, resulting in the recovery of the initial equilibrium state and thus the complete disappearance of the anisotropic scattering signal.

From this comprehensive picture of structural dynamics, the trajectory of the OKE response of liquid acetonitrile can be obtained in terms of the degree of the orientational alignment of the cage molecules (x-axis) and the degree of translational broadening of the intermolecular distance (y-axis), as shown in Figure 4b. From the changes of the RDFs and ODFs along the trajectory, we can learn that (i) the libration and the orientational diffusion are almost exclusively orientational motions, causing no change in the average interatomic distance, and (ii) the interaction-induced motion almost exclusively involves only translation, meaning that the orientational and translational motions are decoupled from each other throughout the entire trajectory. Here we note that while a simple assignment of the character of each motion, whether the motion is of a translational or rotational character, is possible with the polarization-resolved OKE spectroscopy,[21,71,85,86] TRXL provides more comprehensive real-space information on those motions, including the time-dependent changes of the intermolecular distance distribution and the angular orientation of the molecules, as shown in Figure 4. Finally, we note that the OKE-XL signal and time-resolved OKE spectroscopic signal show different dependencies on the concentration of a solution, as discussed in the SI.

CONCLUSION

This work reveals the molecular-level structural origin of OKE and its relaxation dynamics using the structurally sensitive scattering-based technique. By taking advantage of the structural sensitivity of the X-ray scattering probe, we visualized the real-space motions associated with the OKE based on the analysis using a MD simulation. In particular, TRXL can probe the different types of motions selectively, even without the aid of theory, due to the anisotropy of 2D scattering patterns and an extra dimension of the q-domain in the OKE-XL data. This result provides a molecular-level description of the OKE response in real space without the need for theoretical methods. As in the case of the OKE spectroscopic data measured at a series of different temperatures and analyzed with mode-coupling theory, the TRXL measurements of the OKE response can be performed at a series of different temperatures. The analysis of those temperature-dependent TRXL data would reveal how the temperature influences the contributions and kinetics of different types of motions such as libration, interaction-induced motion, and orientational diffusion. We suggest that the fs-TRXL measurement of the molecular motions associated with the OKE can be a powerful tool for studying the ultrafast dynamics of molecular liquids with molecular-level structural details and a femtosecond time resolution.

EXPERIMENTAL SECTION

The TRXL experiment was conducted at the XSS beamline of the Pohang Accelerator Laboratory X-ray Free-Electron Laser (PAL-XFEL). This fourth-generation accelerator provides much shorter and stronger X-ray pulses than the third-generation synchrotrons, enabling the observation of ultrafast dynamics of molecular systems that undergo physical or chemical changes on femtosecond time scales. In this experiment, two short pulses were used to observe the evolution of transiently aligned molecules. One is an optical pump pulse that applies a strong electromagnetic field to the sample to induce the transient photoalignment of liquid molecules (that is, the optical Kerr effect), and the other is an X-ray probe pulse that monitors the process of molecular rearrangement. The TRXL signals were measured while changing the time delay (Δt) between the laser pump and the X-ray probe pulses. A 0.5 mM solution of 4-bromo-4′-(*N*,*N*-diethylamino)-azobenzene (CAS 22700-62-5, HANCHEM, 99.9%) in acetonitrile (Sigma-Aldrich, 99.9%) was prepared as a sample. An open-jet system with a quartz capillary nozzle with an inner diameter of 100 μm was used to continuously provide a stable liquid jet of the sample. The 400 nm laser pulses with a fluence of 1.8 mJ/mm^2 generated by the frequency doubling of the output from the Ti:sapphire laser were used as a pump to induce the transient alignment of the liquid molecules in the sample. The laser was vertically polarized at the sample position. X-ray pulses with a center energy of 12.7 keV were used. The diameters of the laser and X-ray beams focused on the liquid jet were 200 and 30 μm, respectively. The X-ray was horizontally polarized at the sample position. The scattering intensities of the 2D scattering patterns were detected by the Rayonix MX225-HS charge-coupled-device detector (5760 × 5760 pixels, 39 μm pixel size) with the 4 × 4 binning mode. To detect the evolution of the time-resolved X-ray scattering signal, we measured the scattering signals at multiple pump−probe time delays in the range from −450 fs to 100 ps.

ASSOCIATED CONTENT

Supporting Information

The Supporting Information is available free of charge at https://pubs.acs.org/doi/10.1021/jacs.1c06088.

DFT and TDDFT calculations, SANOD to remove a systematic artifact or the contribution of solvent heating, kinetic and lineshape analyses, MD simulations, calculation of theoretical two-dimensional scattering patterns, calculation of theoretical difference scattering curves from MD snapshots, and comparison of fs-TRXL and OKE spectroscopy for probing the OKE response (PDF)

https://doi.org/10.1021/jacs.1c06088
J. Am. Chem. Soc. 2021, 143, 14261−14273

AUTHOR INFORMATION

Corresponding Authors

Hyotcherl Ihee − *Department of Chemistry and KI for the BioCentury, Korea Advanced Institute of Science and Technology (KAIST), Daejeon 34141, Republic of Korea; Center for Nanomaterials and Chemical Reactions, Institute for Basic Science (IBS), Daejeon 34141, Republic of Korea;* orcid.org/0000-0003-0397-5965; Email: hyotcherl.ihee@kaist.ac.kr

Jeongho Kim − *Department of Chemistry, Inha University, Incheon 22212, Republic of Korea;* orcid.org/0000-0003-4085-293X; Email: jkim5@inha.ac.kr

Authors

Hosung Ki − *Department of Chemistry and KI for the BioCentury, Korea Advanced Institute of Science and Technology (KAIST), Daejeon 34141, Republic of Korea; Center for Nanomaterials and Chemical Reactions, Institute for Basic Science (IBS), Daejeon 34141, Republic of Korea;* orcid.org/0000-0001-8273-6596

Seungjoo Choi − *Department of Chemistry, Inha University, Incheon 22212, Republic of Korea;* orcid.org/0000-0003-1154-4698

Jungmin Kim − *Department of Chemistry and KI for the BioCentury, Korea Advanced Institute of Science and Technology (KAIST), Daejeon 34141, Republic of Korea; Center for Nanomaterials and Chemical Reactions, Institute for Basic Science (IBS), Daejeon 34141, Republic of Korea*

Eun Hyuk Choi − *Department of Chemistry and KI for the BioCentury, Korea Advanced Institute of Science and Technology (KAIST), Daejeon 34141, Republic of Korea; Center for Nanomaterials and Chemical Reactions, Institute for Basic Science (IBS), Daejeon 34141, Republic of Korea*

Seonggon Lee − *Department of Chemistry and KI for the BioCentury, Korea Advanced Institute of Science and Technology (KAIST), Daejeon 34141, Republic of Korea; Center for Nanomaterials and Chemical Reactions, Institute for Basic Science (IBS), Daejeon 34141, Republic of Korea*

Yunbeom Lee − *Department of Chemistry and KI for the BioCentury, Korea Advanced Institute of Science and Technology (KAIST), Daejeon 34141, Republic of Korea; Center for Nanomaterials and Chemical Reactions, Institute for Basic Science (IBS), Daejeon 34141, Republic of Korea*

Kihwan Yoon − *Department of Chemistry, The Catholic University of Korea, Bucheon 14662, Republic of Korea*

Chi Woo Ahn − *Department of Chemistry and KI for the BioCentury, Korea Advanced Institute of Science and Technology (KAIST), Daejeon 34141, Republic of Korea; Center for Nanomaterials and Chemical Reactions, Institute for Basic Science (IBS), Daejeon 34141, Republic of Korea*

Doo-Sik Ahn − *Department of Chemistry and KI for the BioCentury, Korea Advanced Institute of Science and Technology (KAIST), Daejeon 34141, Republic of Korea; Center for Nanomaterials and Chemical Reactions, Institute for Basic Science (IBS), Daejeon 34141, Republic of Korea*

Jae Hyuk Lee − *Pohang Accelerator Laboratory, Pohang 37673, Republic of Korea*

Jaeku Park − *Pohang Accelerator Laboratory, Pohang 37673, Republic of Korea*

Intae Eom − *Pohang Accelerator Laboratory, Pohang 37673, Republic of Korea*

Minseok Kim − *Pohang Accelerator Laboratory, Pohang 37673, Republic of Korea*

Sae Hwan Chun − *Pohang Accelerator Laboratory, Pohang 37673, Republic of Korea*

Joonghan Kim − *Department of Chemistry, The Catholic University of Korea, Bucheon 14662, Republic of Korea;* orcid.org/0000-0002-7783-0200

Complete contact information is available at: https://pubs.acs.org/10.1021/jacs.1c06088

Author Contributions

[∇]H.K. and S.C. contributed equally to this work.

Notes

The authors declare no competing financial interest.

ACKNOWLEDGMENTS

This work was supported by the Institute for Basic Science (IBS-R004). This work was supported by the Basic Science Research Program through the National Research Foundation of Korea (NRF) funded by the Ministry of Science, ICT, and Future Planning (nos. 2016R1E1A1A01941978 and 2020K1A3A7A09080401). The experiment was performed at the XSS beamline of PAL-XFEL (proposal nos. 2019-1st-XSS-011 and 2019-2nd-XSS-013) funded by the Ministry of Science and the ICT of Korea.

REFERENCES

(1) Duguay, M. A.; Hansen, J. W. An ultrafast light gate. *Appl. Phys. Lett.* **1969**, *15*, 192−194.

(2) Ho, P. P.; Alfano, R. R. Optical Kerr effect in liquids. *Phys. Rev. A: At., Mol., Opt. Phys.* **1979**, *20*, 2170−2187.

(3) Righini, R. Ultrafast Optical Kerr Effect in Liquids and Solids. *Science* **1993**, *262*, 1386−1390.

(4) Palese, S.; Schilling, L.; Miller, R. J. D.; Staver, P. R.; Lotshaw, W. T. Femtosecond optical Kerr effect studies of water. *J. Phys. Chem.* **1994**, *98*, 6308−6316.

(5) Fisher, R. A.; Kelley, P. L.; Gustafson, T. K. Subpicosecond pulse generation using the optical Kerr effect. *Appl. Phys. Lett.* **1969**, *14*, 140−143.

(6) Loughnane, B. J.; Scodinu, A.; Farrer, R. A.; Fourkas, J. T.; Mohanty, U. Exponential intermolecular dynamics in optical Kerr effect spectroscopy of small-molecule liquids. *J. Chem. Phys.* **1999**, *111*, 2686−2694.

(7) Park, S.; Flanders, B. N.; Shang, X.; Westervelt, R. A.; Kim, J.; Scherer, N. F. Solvent intermolecular polarizability response in solvation. *J. Chem. Phys.* **2003**, *118*, 3917−3920.

(8) Zhong, Q.; Fourkas, J. T. Optical Kerr Effect Spectroscopy of Simple Liquids. *J. Phys. Chem. B* **2008**, *112*, 15529−15539.

(9) Park, S.; Kim, J.; Scherer, N. F. Two-dimensional measurements of the solvent structural relaxation dynamics in dipolar solvation. *Phys. Chem. Chem. Phys.* **2012**, *14*, 8116−8122.

(10) Kinoshita, S.; Kai, Y.; Ariyoshi, T.; Shimada, Y. Low frequency modes probed by time-domain optical Kerr effect spectroscopy. *Int. J. Mod. Phys. B* **1996**, *10*, 1229−1272.

(11) Cho, M.; Rosenthal, S. J.; Scherer, N. F.; Ziegler, L. D.; Fleming, G. R. Ultrafast solvent dynamics: Connection between time resolved fluorescence and optical Kerr measurements. *J. Chem. Phys.* **1992**, *96*, 5033−5038.

(12) Maroncelli, M.; Kumar, V. P.; Papazyan, A. A simple interpretation of polar solvation dynamics. *J. Phys. Chem.* **1993**, *97*, 13−17.

(13) Raineri, F. O.; Friedman, H. L. The power law aspect of solvation dynamics, based on the convolutionless generalized Langevin equation. *J. Chem. Phys.* **1994**, *101*, 6111−6115.

(14) Ladanyi, B. M.; Klein, S. Contributions of rotation and translation to polarizability anisotropy and solvation dynamics in acetonitrile. *J. Chem. Phys.* **1996**, *105*, 1552−1561.

(15) Underwood, D. F.; Blank, D. A. Ultrafast solvation dynamics: A view from the solvent's perspective using a novel resonant-pump, nonresonant-probe technique. *J. Phys. Chem. A* **2003**, *107*, 956−961.
(16) Schmidtke, S. J.; Underwood, D. F.; Blank, D. A. Probing excited-state dynamics and intramolecular proton transfer in 1-acylaminoanthraquinones via the intermolecular solvent response. *J. Phys. Chem. A* **2005**, *109*, 7033−7045.
(17) Smith, N. A.; Lin, S.; Meech, S. R.; Yoshihara, K. Ultrafast optical Kerr effect and solvation dynamics of liquid aniline. *J. Phys. Chem. A* **1997**, *101*, 3641−3645.
(18) Ladanyi, B. M.; Stratt, R. M. Short-time dynamics of solvation: Linear solvation theory for polar solvents. *J. Phys. Chem.* **1995**, *99*, 2502−2511.
(19) Stratt, R. M.; Maroncelli, M. Nonreactive dynamics in solution: The emerging molecular view of solvation dynamics and vibrational relaxation. *J. Phys. Chem.* **1996**, *100*, 12981−12996.
(20) Chang, Y. J.; Castner, E. W. Intermolecular dynamics of substituted benzene and cyclohexane liquids, studied by femtosecond nonlinear-optical polarization spectroscopy. *J. Phys. Chem.* **1996**, *100*, 3330−3343.
(21) Hunt, N. T.; Meech, S. R. Orientational and interaction induced dynamics in the isotropic phase of a liquid crystal: Polarization resolved ultrafast optical Kerr effect spectroscopy. *J. Chem. Phys.* **2004**, *120*, 10828−10836.
(22) Ladanyi, B. M.; Maroncelli, M. Mechanisms of solvation dynamics of polyatomic solutes in polar and nondipolar solvents: A simulation study. *J. Chem. Phys.* **1998**, *109*, 3204−3221.
(23) Sun, X.; Stratt, R. M. How a solute-pump/solvent-probe spectroscopy can reveal structural dynamics: Polarizability response spectra as a two-dimensional solvation spectroscopy. *J. Chem. Phys.* **2013**, *139*, 044506.
(24) Ryu, S.; Stratt, R. M. A case study in the molecular interpretation of optical Kerr effect spectra: Instantaneous-normal-mode analysis of the OKE spectrum of liquid benzene. *J. Phys. Chem. B* **2004**, *108*, 6782−6795.
(25) Idrissi, A.; Bartolini, P.; Ricci, M.; Righini, R. Time resolved optical Kerr effect analysis of urea−water system. *J. Chem. Phys.* **2001**, *114*, 6774−6780.
(26) Sonoda, M. T.; Vechi, S. M.; Skaf, M. S. A simulation study of the optical Kerr effect in liquid water. *Phys. Chem. Chem. Phys.* **2005**, *7*, 1176−1180.
(27) Ngai, K. L.; Paluch, M. Inference of the evolution from caged dynamics to cooperative relaxation in glass-formers from dielectric relaxation data. *J. Phys. Chem. B* **2003**, *107*, 6865−6872.
(28) Taschin, A.; Bartolini, P.; Eramo, R.; Righini, R.; Torre, R. Optical Kerr effect of liquid and supercooled water: The experimental and data analysis perspective. *J. Chem. Phys.* **2014**, *141*, 084507.
(29) Taschin, A.; Bartolini, P.; Eramo, R.; Righini, R.; Torre, R. Evidence of two distinct local structures of water from ambient to supercooled conditions. *Nat. Commun.* **2013**, *4*, 2401.
(30) Kim, K. H.; Kim, J. G.; Nozawa, S.; Sato, T.; Oang, K. Y.; Kim, T. W.; Ki, H.; Jo, J.; Park, S.; Song, C.; Sato, T.; Ogawa, K.; Togashi, T.; Tono, K.; Yabashi, M.; Ishikawa, T.; Kim, J.; Ryoo, R.; Kim, J.; Ihee, H.; Adachi, S. Direct observation of bond formation in solution with femtosecond X-ray scattering. *Nature* **2015**, *518*, 385−389.
(31) Biasin, E.; van Driel, T. B.; Kjær, K. S.; Dohn, A. O.; Christensen, M.; Harlang, T.; Chabera, P.; Liu, Y.; Uhlig, J.; Pápai, M.; Németh, Z.; Hartsock, R.; Liang, W.; Zhang, J.; Alonso-Mori, R.; Chollet, M.; Glownia, J. M.; Nelson, S.; Sokaras, D.; Assefa, T. A.; Britz, A.; Galler, A.; Gawelda, W.; Bressler, C.; Gaffney, K. J.; Lemke, H. T.; Møller, K. B.; Nielsen, M. M.; Sundström, V.; Vankó, G.; Wärnmark, K.; Canton, S. E.; Haldrup, K. Femtosecond x-ray scattering study of ultrafast photoinduced structural dynamics in solvated $[Co(terpy)_2]^{2+}$. *Phys. Rev. Lett.* **2016**, *117*, 013002.
(32) Kim, K. H.; Kim, J. G.; Oang, K. Y.; Kim, T. W.; Ki, H.; Jo, J.; Kim, J.; Sato, T.; Nozawa, S.; Adachi, S.; Ihee, H. Femtosecond X-ray solution scattering reveals that bond formation mechanism of a gold trimer complex is independent of excitation wavelength. *Struct. Dyn.* **2016**, *3*, 043209.
(33) Biasin, E.; van Driel, T. B.; Levi, G.; Laursen, M. G.; Dohn, A. O.; Moltke, A.; Vester, P.; Hansen, F. B. K.; Kjaer, K. S.; Harlang, T.; Hartsock, R.; Christensen, M.; Gaffney, K. J.; Henriksen, N. E.; Møller, K. B.; Haldrup, K.; Nielsen, M. M. Anisotropy enhanced X-ray scattering from solvated transition metal complexes. *J. Synchrotron Radiat.* **2018**, *25*, 306−315.
(34) Kim, J. G.; Nozawa, S.; Kim, H.; Choi, E. H.; Sato, T.; Kim, T. W.; Kim, K. H.; Ki, H.; Kim, J.; Choi, M.; Lee, Y.; Heo, J.; Oang, K. Y.; Ichiyanagi, K.; Fukaya, R.; Lee, J. H.; Park, J.; Eom, I.; Chun, S. H.; Kim, S.; Kim, M.; Katayama, T.; Togashi, T.; Owada, S.; Yabashi, M.; Lee, S. J.; Lee, S.; Ahn, C. W.; Ahn, D.-S.; Moon, J.; Choi, S.; Kim, J.; Joo, T.; Kim, J.; Adachi, S.; Ihee, H. Mapping the emergence of molecular vibrations mediating bond formation. *Nature* **2020**, *582*, 520−524.
(35) Kim, K. H.; Späh, A.; Pathak, H.; Yang, C.; Bonetti, S.; Amann-Winkel, K.; Mariedahl, D.; Schlesinger, D.; Sellberg, J. A.; Mendez, D.; van der Schot, G.; Hwang, H. Y.; Clark, J.; Shigeki, O.; Tadashi, T.; Harada, Y.; Ogasawara, H.; Katayama, T.; Nilsson, A.; Perakis, F. Anisotropic x-ray scattering of transiently oriented water. *Phys. Rev. Lett.* **2020**, *125*, 076002.
(36) Biasin, E.; Fox, Z. W.; Andersen, A.; Ledbetter, K.; Kjær, K. S.; Alonso-Mori, R.; Carlstad, J. M.; Chollet, M.; Gaynor, J. D.; Glownia, J. M.; Hong, K.; Kroll, T.; Lee, J. H.; Liekhus-Schmaltz, C.; Reinhard, M.; Sokaras, D.; Zhang, Y.; Doumy, G.; March, A. M.; Southworth, S. H.; Mukamel, S.; Gaffney, K. J.; Schoenlein, R. W.; Govind, N.; Cordones, A. A.; Khalil, M. Direct observation of coherent femtosecond solvent reorganization coupled to intramolecular electron transfer. *Nat. Chem.* **2021**, *13*, 343−349.
(37) Choi, E. H.; Kim, J. G.; Kim, J.; Ki, H.; Lee, Y.; Lee, S.; Yoon, K.; Kim, J.; Kim, J.; Ihee, H. Filming ultrafast roaming-mediated isomerization of bismuth triiodide in solution. *Nat. Commun.* **2021**, *12*, 4732.
(38) Christensen, M.; Haldrup, K.; Bechgaard, K.; Feidenhans'l, R.; Kong, Q.; Cammarata, M.; Russo, M. L.; Wulff, M.; Harrit, N.; Nielsen, M. M. Time-resolved x-ray scattering of an electronically excited state in solution. Structure of the $^3A_{2u}$ state of tetrakis-μ-pyrophosphitodiplatinate(II). *J. Am. Chem. Soc.* **2009**, *131*, 502−508.
(39) Kim, T. K.; Lee, J. H.; Wulff, M.; Kong, Q.; Ihee, H. Spatiotemporal kinetics in solution studied by time-resolved x-ray liquidography (solution scattering). *ChemPhysChem* **2009**, *10*, 1958−1980.
(40) Cho, H. S.; Dashdorj, N.; Schotte, F.; Graber, T.; Henning, R.; Anfinrud, P. Protein structural dynamics in solution unveiled via 100-ps time-resolved x-ray scattering. *Proc. Natl. Acad. Sci. U. S. A.* **2010**, *107*, 7281−7286.
(41) Haldrup, K.; Christensen, M.; Nielsen, M. M. Analysis of time-resolved X-ray scattering data from solution-state systems. *Acta Crystallogr., Sect. A: Found. Crystallogr.* **2010**, *66*, 261−269.
(42) Ihee, H.; Wulff, M.; Kim, J.; Adachi, S. Ultrafast X-ray scattering: structural dynamics from diatomic to protein molecules. *Int. Rev. Phys. Chem.* **2010**, *29*, 453−520.
(43) Malmerberg, E.; Omran, Z.; Hub, J. S.; Li, X.; Katona, G.; Westenhoff, S.; Johansson, L. C.; Andersson, M.; Cammarata, M.; Wulff, M.; van der Spoel, D.; Davidsson, J.; Specht, A.; Neutze, R. Time-resolved WAXS reaveals accelerated conformational changes in iodoretinal-substituted proteorhodopsin. *Biophys. J.* **2011**, *101*, 1345−1353.
(44) Kim, K. H.; Ki, H.; Lee, J. H.; Park, S.; Kong, Q.; Kim, J.; Kim, J.; Wulff, M.; Ihee, H. Solvent-dependent structure of molecular iodine probed by picosecond X-ray solution scattering. *Phys. Chem. Chem. Phys.* **2015**, *17*, 8633−8637.
(45) Biasin, E. *Structural dynamics of solvated metal complexes with anisotropy-enhanced X-ray scattering.*. Ph.D. Thesis, Technical University of Denmark, Copenhagen, Denmark, 2016.
(46) Haldrup, K.; Dohn, A. O.; Shelby, M. L.; Mara, M. W.; Stickrath, A. B.; Harpham, M. R.; Huang, J.; Zhang, X.; Møller, K. B.; Chakraborty, A.; Castellano, F. N.; Tiede, D. M.; Chen, L. X. Butterfly deformation modes in a photoexcited pyrazolate-bridged Pt complex

https://doi.org/10.1021/jacs.1c06088
J. Am. Chem. Soc. 2021, 143, 14261−14273

measured by time-resolved x-ray scattering in solution. *J. Phys. Chem. A* **2016**, *120*, 7475−7483.
(47) Ki, H.; Oang, K. Y.; Kim, J.; Ihee, H. Ultrafast x-ray crystallography and liquidography. *Annu. Rev. Phys. Chem.* **2017**, *68*, 473−497.
(48) Kjær, K. S.; van Driel, T. B.; Harlang, T. C. B.; Kunnus, K.; Biasin, E.; Ledbetter, K.; Hartsock, R. W.; Reinhard, M. E.; Koroidov, S.; Li, L.; Laursen, M. G.; Hansen, F. B.; Vester, P.; Christensen, M.; Haldrup, K.; Nielsen, M. M.; Dohn, A. O.; Pápai, M. I.; Møller, K. B.; Chabera, P.; Liu, Y.; Tatsuno, H.; Timm, C.; Jarenmark, M.; Uhlig, J.; Sundstöm, V.; Wärnmark, K.; Persson, P.; Németh, Z.; Szemes, D. S.; Bajnóczi, É.; Vankó, G.; Alonso-Mori, R.; Glownia, J. M.; Nelson, S.; Sikorski, M.; Sokaras, D.; Canton, S. E.; Lemke, H. T.; Gaffney, K. J. Finding intersections between electronic excited state potential energy surfaces with simultaneous ultrafast x-ray scattering and spectroscopy. *Chem. Sci.* **2019**, *10*, 5749−5760.
(49) Ihee, H.; Lorenc, M.; Kim, T. K.; Kong, Q. Y.; Cammarata, M.; Lee, J. H.; Bratos, S.; Wulff, M. Ultrafast x-ray diffraction of transient molecular structures in solution. *Science* **2005**, *309*, 1223−1227.
(50) Kim, J.; Kim, K. H.; Kim, J. G.; Kim, T. W.; Kim, Y.; Ihee, H. Anisotropic picosecond x-ray solution scattering from photoselectively aligned protein molecules. *J. Phys. Chem. Lett.* **2011**, *2*, 350−356.
(51) Kim, J. G.; Kim, K. H.; Oang, K. Y.; Kim, T. W.; Ki, H.; Jo, J.; Kim, J.; Sato, T.; Nozawa, S.; Adachi, S.; Ihee, H. Rotational dephasing of a gold complex probed by anisotropic femtosecond x-ray solution scattering using an x-ray free-electron laser. *J. Phys. B: At., Mol. Opt. Phys.* **2015**, *48*, 244005.
(52) Cammarata, M.; Lorenc, M.; Kim, T. K.; Lee, J. H.; Kong, Q. Y.; Pontecorvo, E.; Lo Russo, M.; Schiró, G.; Cupane, A.; Wulff, M.; Ihee, H. Impulsive solvent heating probed by picosecond x-ray diffraction. *J. Chem. Phys.* **2006**, *124*, 124504.
(53) Kjær, K. S.; van Driel, T. B.; Kehres, J.; Haldrup, K.; Khakhulin, D.; Bechgaard, K.; Cammarata, M.; Wulff, M.; Sørensen, T. J.; Nielsen, M. M. Introducing a standard method for experimental determination of the solvent response in laser pump, X-ray probe time-resolved wide-angle X-ray scattering experiments on system in solution. *Phys. Chem. Chem. Phys.* **2013**, *15*, 15003−15016.
(54) Baskin, J. S.; Zewail, A. H. Ultrafast electron diffraction: Oriented molecular structures in space and time. *ChemPhysChem* **2005**, *6*, 2261−2276.
(55) Baskin, J. S.; Zewail, A. H. Oriented ensembles in ultrafast electron diffraction. *ChemPhysChem* **2006**, *7*, 1562−1574.
(56) Lorenz, U.; Møller, K. B.; Henriksen, N. E. On the interpretation of time-resolved anisotropic diffraction patterns. *New J. Phys.* **2010**, *12*, 113022.
(57) Panman, M. R.; Biasin, E.; Berntsson, O.; Hermann, M.; Niebling, S.; Hughes, A. J.; Kübel, J.; Atkovska, K.; Gustavsson, E.; Nimmrich, A.; Dohn, A. O.; Laursen, M.; Zederkof, D. B.; Honarfar, A.; Tono, K.; Katayama, T.; Owada, S.; van Driel, T. B.; Kjaer, K.; Nielsen, M. M.; Davidsson, J.; Uhlig, J.; Haldrup, K.; Hub, J. S.; Westenhoff, S. Observing the structural evolution in the photodissociation of diiodomethane with femtosecond solution x-ray scattering. *Phys. Rev. Lett.* **2020**, *125*, 226001.
(58) Jimenez, R.; Fleming, G. R.; Kumar, P. V.; Maroncelli, M. Femtosecond solvation dynamics of water. *Nature* **1994**, *369*, 471−473.
(59) Yu, J.; Earvolino, P.; Berg, M. Solvent-electronic state interactions measured from the glassy to the liquid state. II. Fluorescence line narrowing spectroscopy in glycerol. *J. Chem. Phys.* **1992**, *96*, 8750−8756.
(60) Joo, T.; Jia, Y.; Fleming, G. R. Ultrafast liquid dynamics studied by third and fifth order three pulse photon echoes. *J. Chem. Phys.* **1995**, *102*, 4063−4068.
(61) Fleming, G. R.; Cho, M. Chromophore-solvent dynamics. *Annu. Rev. Phys. Chem.* **1996**, *47*, 109−134.
(62) de Boeij, W. P.; Pshenichnikov, M. S.; Wiersma, D. A. Ultrafast solvation dynamics explored by femtosecond photon echo spectroscopies. *Annu. Rev. Phys. Chem.* **1998**, *49*, 99−123.
(63) Fourkas, J. T.; Berg, M. Temperature-dependent ultrafast solvation dynamics in a completely nonpolar system. *J. Chem. Phys.* **1993**, *98*, 7773−7785.
(64) Bagchi, B.; Jana, B. Solvation dynamics in dipolar liquids. *Chem. Soc. Rev.* **2010**, *39*, 1936−1954.
(65) Moran, A. M.; Park, S.; Scherer, N. F. Polarizability response spectroscopy: Formalism and simulation of ultrafast dynamics in solvation. *Chem. Phys.* **2007**, *341*, 344−356.
(66) Moreno, J.; Gerecke, M.; Dobryakov, A. L.; Ioffe, I. N.; Granovsky, A. A.; Bléger, D.; Hecht, S.; Kovalenko, S. A. Two-photon-induced versus one-photon-induced isomerization dynamics of a bistable azobenzene derivative in solution. *J. Phys. Chem. B* **2015**, *119*, 12281−12288.
(67) Quick, M.; Dobryakov, A. L.; Gerecke, M.; Richter, C.; Berndt, F.; Ioffe, I. N.; Granovsky, A. A.; Mahrwald, R.; Ernsting, N. P.; Kovalenko, S. A. Photoisomerization dynamics and pathways of trans- and cis-azobenzene in solution from broadband femtosecond spectroscopies and calculations. *J. Phys. Chem. B* **2014**, *118*, 8756−8771.
(68) Ki, H.; Lee, Y.; Choi, E. H.; Lee, S.; Ihee, H. SVD-aided non-orthogonal decomposition (SANOD) method to exploit prior knowledge of spectral components in the analysis of time-resolved data. *Struct. Dyn.* **2019**, *6*, 024303.
(69) Oang, K. Y.; Yang, C.; Muniyappan, S.; Kim, J.; Ihee, H. SVD-aided pseudo principal-component analysis: A new method to speed up and improve determination of the optimum kinetic model from time-resolved data. *Struct. Dyn.* **2017**, *4*, 044013.
(70) Passino, S. A.; Nagasawa, Y.; Joo, T.; Fleming, G. R. Three-pulse echo peak shift studies of polar solvation dynamics. *J. Phys. Chem. A* **1997**, *101*, 725−731.
(71) Fecko, C. J.; Eaves, J. D.; Tokmakoff, A. Isotropic and anisotropic Raman scattering from molecular liquids measured by spatially masked optical Kerr effect spectroscopy. *J. Chem. Phys.* **2002**, *117*, 1139−1154.
(72) Kakinuma, S.; Shirota, H. Femtosecond Raman-induced Kerr effect study of temperature-dependent intermolecular dynamics in molten bis(trifluoromethylsulfonyl)amide salts: Effects of cation species. *J. Phys. Chem. B* **2018**, *122*, 6033−6047.
(73) Kakinuma, S.; Shirota, H. Femtosecond Raman-induced Kerr effect study of temperature-dependent intermolecular dynamics in pyrrolidinium-based ionic liquids: Effects of anion species. *J. Phys. Chem. B* **2019**, *123*, 1307−1323.
(74) Marrucci, L.; Paparo, D.; Abbate, G.; Santamato, E.; Kreuzer, M.; Lehnert, P.; Vogeler, T. Enhanced optical nonlinearity by photoinduced molecular orientation in absorbing liquids. *Phys. Rev. A: At., Mol., Opt. Phys.* **1998**, *58*, 4926−4936.
(75) Paparo, D.; Marrucci, L.; Abbate, G.; Santamato, E.; Kreuzer, M.; Lehnert, P.; Vogeler, T. Molecular-field-enhanced optical Kerr effect in absorbing liquids. *Phys. Rev. Lett.* **1997**, *78*, 38−41.
(76) Pothoczki, S.; Pusztai, L. Intermolecular orientations in liquid acetonitrile: New insights based on diffraction measurements and all-atom simulations. *J. Mol. Liq.* **2017**, *225*, 160−166.
(77) Novoa, J. J.; Mota, F.; del Valle, C. P.; Planas, M. Structure of the first solvation shell of the hydroxide anion. A model study using $OH^-(H_2O)_n$ (n = 4, 5, 6, 7, 11, 17) clusters. *J. Phys. Chem. A* **1997**, *101*, 7842−7853.
(78) Wang, C. I.; Hua, C. C.; Chen, S. A. Dynamic solvation shell and solubility of C_{60} in organic solvents. *J. Phys. Chem. B* **2014**, *118*, 9964−9973.
(79) Baldwin, R. L. Dynamic hydration shell restores Kauzmann's 1959 explanation of how the hydrophobic factor drives protein folding. *Proc. Natl. Acad. Sci. U. S. A.* **2014**, *111*, 13052−13056.
(80) Davis, J. G.; Gierszal, K. P.; Wang, P.; Ben-Amotz, D. Water structural transformation at molecular hydrophobic interfaces. *Nature* **2012**, *491*, 582−585.
(81) Henao, A.; Busch, S.; Guardia, E.; Tamarit, J. L.; Pardo, L. C. The structure of liquid water beyond the first hydration shell. *Phys. Chem. Chem. Phys.* **2016**, *18*, 19420−19425.

https://doi.org/10.1021/jacs.1c06088
J. Am. Chem. Soc. 2021, 143, 14261−14273

(82) Thoma, S. L. J.; Krauss, S. W.; Eckardt, M.; Chater, P.; Zobel, M. Atomic insight into hydration shells around facetted nanoparticles. *Nat. Commun.* **2019**, *10*, 995.
(83) Cordeiro, J. M. M.; Soper, A. K. A hybrid neutron diffraction and computer simulation study on the solvation of *N*-methylformamide in dimethylsulfoxide. *J. Chem. Phys.* **2013**, *138*, 044502.
(84) Heisler, I. A.; Meech, S. R. Low-frequency modes of aqueous alkali halide solutions: Glimpsing the hydrogen bonding vibration. *Science* **2010**, *327*, 857−860.
(85) Khalil, M.; Golonzka, O.; Demirdöven, N.; Fecko, C. J.; Tokmakoff, A. Polarization-selective femtosecond Raman spectroscopy of isotropic and anisotropic vibrational dynamics in liquids. *Chem. Phys. Lett.* **2000**, *321*, 231−237.
(86) Heisler, I. A.; Meech, S. R. Polarization-resolved ultrafast polarizability relaxation in polar aromatic liquids. *J. Phys. Chem. B* **2008**, *112*, 12976−12984.

https://doi.org/10.1021/jacs.1c06088
J. Am. Chem. Soc. 2021, 143, 14261−14273